applied sciences

MDPI

Article

Analysis of the Driving Altitude and Ambient Temperature Impact on the Conversion Efficiency of Oxidation Catalysts

José Ramón Serrano, Pedro Piqueras *, Enrique José Sanchis and Bárbara Diesel

CMT-Motores Térmicos, Universitat Politècnica de València, Camino de Vera s/n, 46022 Valencia, Spain; jrserran@mot.upv.es (J.R.S.); ensanpac@mot.upv.es (E.J.S.); bardicos@mot.upv.es (B.D.)
* Correspondence: pedpicab@mot.upv.es; Tel.: +34-963877650

Abstract: Worldwide emission standards are extending their requirements to cover engine operation under extreme ambient conditions and fill the gap between the type-approval and real driving conditions. The new ambient boundaries affect the engine performance and raw emissions as well as the efficiency of the exhaust aftertreatment systems. This study evaluates the impact of high altitude and low ambient temperature on the light-off temperature and conversion efficiency of an oxidation catalyst. The results are compared in a common range of exhaust mass flow and temperature with the baseline sea-level operation at 20 °C. A reduction of CO and HC conversion efficiencies was found at 2500 m and −7 °C, with a relevant increase of the light-off temperature for both of the pollutants. The analysis of the experimental data was complemented with the use of a catalyst model to identify the causes leading to the deterioration of the CO and HC light-off. The use of the model allowed for identifying, for the same exhaust mass flow and temperature, the contributions to the variation of conversion efficiency caused by the change in engine-out emissions and tailpipe pressure, which are, in turn, manifested in the variation of the reactants partial pressure and dwell time as governing parameters.

Keywords: internal combustion engine; exhaust aftertreatment system; conversion efficiency; altitude; ambient temperature; light-off

Citation: Serrano, J.R.; Piqueras, P.; Sanchis, E.J.; Diesel, B. Analysis of the Driving Altitude and Ambient Temperature Impact on the Conversion Efficiency of Oxidation Catalysts. *Appl. Sci.* **2021**, *11*, 1283. https://doi.org/10.3390/app11031283

Academic Editor: Antonio Bartolomeo
Received: 29 December 2020
Accepted: 27 January 2021
Published: 30 January 2021

1. Introduction

Increasingly tightened emission standards progressively reflect the societal demand for clean sustainable transport [1]. This process is making the optimization of the internal combustion engine not sufficient in meeting the new requirements and demanding a robust matching between engine and exhaust aftertreatment system (ATS) [2]. In Europe, the current regulations include real driving emission (RDE) tests for passenger cars and light duty vehicles with the aim of reducing the gap between the emissions during vehicle tests at type-approval and real-life ones. These tests complement the lab-based one, i.e., the World harmonized Light vehicle Test Cycle (WLTC) as type-approval test of the Worldwide harmonized Light vehicle Test Procedure (WLTP). In compliance with these regulations, the new generation of diesel engines still guarantees the most robust alternative for low CO_2 emissions of internal combustion engines, which encourages further research on this topic.

RDE tests include the ambient conditions as additional boundaries. In particular, moderate and extended ranges are defined [3], while considering altitude from 0 to 700 m and ambient temperature from 0 °C to 30 °C in the moderate case and altitude between 700 and 1300 m with temperature ranging from −7 °C to 35 °C for the extended conditions. These ranges bring the regulations closer to real-life, since about 60% of the European population live in or close to massifs and 20% in mountain municipalities [4]. Furthermore, cities that are located at high altitude face severe temperatures in winter, which justifies considering the ambient temperature in combination with altitude [5]. Similar boundaries

are being adopted in other countries, like China, where the altitude range is extended until 2400 m, or India, which defines a temperature range shifted toward warmer conditions (8–45 °C).

Under this context, the effect of extreme ambient conditions on the engine performance must be faced, due to their potential negative impact on emissions and fuel consumption [6]. Ko et al. [7] showed that a low ambient temperature highly affected NO_x and CO emissions in a Euro 6 diesel engine. Luján et al. [8] also discussed this result, who also found a penalty in fuel consumption close to 10% running driving cycles at −7 °C. Despite the interest for the combination of high-pressure (HP) and low-pressure (LP) exhaust gas recirculation (EGR) [9], extremely cold temperatures can also lead to a decrease the EGR rate, as discussed by Galindo et al. [10] regarding condensation in the LP-EGR path. In a similar way, operation at high altitude penalizes the engine performance concerning the combustion [11] and gas exchange processes [12], as well as emissions [13]. In this regard, Table 1 summarizes the contributions of different works from the literature regarding the impact of the driving altitude and ambient temperature on the pollutant emissions, including the main conclusion of this work, as discussed later in detail.

Table 1. Comparison of results reported in the literature regarding the impact of altitude and ambient temperature on emissions.

Reference	Engine	Legislation	Operating Conditions	Contribution
Luján et al. [6]	Diesel 1.6 L	Euro 5	0 m & 20 °C; 0 m & −7 °C	WLTC. Higher engine-out emissions at −7° than at 20 °C along with decrease of DOC conversion efficiency.
Ko et al. [7]	Diesel 2.2 L	Euro 6	0 m & 23 °C, 14 °C and 5 °C	NEDC and WLTC. Higher NO_x and CO emissions at low ambient temperature.
Bermúdez et al. [12]	Diesel 2.0 L	Euro 4	150 m to 3000 m & Ambient temperature n/a	NEDC. Increase on CO, HC and NO_x emissions with altitude.
Ramos et al. [13]	Diesel 2.0 L; Biodiesel 2.0 L; GTL 2.0 L.	Euro 4	0 m to 2500 m, ambient temperature n/a	WLTP + RDE-LDV test. At high altitude NO_x emissions were higher. Effect of fuels agrees with cetane number.
Wang et al. [14]	Diesel 2.8 L	Chinese National III	1000 m & 25 °C; 2400 m & 27 °C; 3200 m & 19 °C	RDE test. Increase of CO, HC and PM with altitude. Higher NO_x emissions at 2400 m than at 1000 m, but lower at 3200 m.
Wang et al. [15]	Diesel 2.0 L	China IV	30 m to 2990 m & 20 °C to 33 °C	RDE test under regulation requirements (1200 m/100 km). Higher CO and PN emissions in altitude but lower NO_x.
Giraldo et al. [16]	Diesel 10.8 L	US EPA 2004	2200 m to 3313 m & 20 °C	RDE test w/o catalytic converter. Values for CO higher than allowed by the legislation.
McCaffery et al. [17]	GDI 2017 2.0 L; GDI 2017 1.5 L; GDI 2018 3.6 L	Tier 3	0 m to 1524 m, ambient temperature n/a	RDE test. Higher PM emissions in altitude. PM reduction by adding catalyzed GPF.
Current work	Diesel 1.6 L	Euro 6d-Temp	0 m & 20 °C; 2500 m & −7 °C	Steady-state conditions. Reduction of CO and HC conversion efficiencies at 2500 m and −7 °C and increase of the light-off temperature.

To this extent, the effect of the environmental conditions on the engine operation also modifies the boundary conditions of the ATS. The exhaust temperature is the main parameter governing the ATS response [18]. Thus, numerous efforts have been conducted for reducing the long warm-up periods [19] looking for faster catalyst light-off. Arnau et al. explored engine-based techniques, such as exhaust line thermal insulation [20] and variable valve timing [21] in diesel engines as a way to increase the exhaust temperature during transient operation. Regarding ATS focused solutions, Serrano et al. [22] discussed the potential and limitations of pre-turbine small-sized catalysts in accelerating the catalyst activation under real driving conditions. Hamedi et al. [23] evaluated the capability to keep the catalyst warm during low temperature periods while using phase change materials. The results showed the interest for this technology in increasing the conversion efficiency in recurrent cold-start cases, as those in hybrid vehicles [24].

However, thermal solutions are not only justified by the increasing periods at low temperature in incoming powertrain systems, but also by the variability of the light-off temperature, which is not the same in all of the operating conditions. ATS boundary conditions, such as pollutants mole fraction or dwell time [25], vary the light-off response of the catalysts [26]. In particular, the exhaust pressure dependence on the driving altitude is reflected in a relevant variation of the pollutants' partial pressure. The volumetric flow rate of the exhaust gas also suffers a direct variation and, consequently, the flow dwell time [27]. The dwell time increase improves the mass transfer of the pollutants toward the catalyst active sites, which implies higher conversion efficiency [28] and a reduction of the light-off temperature [29]. On the contrary, an increase in the volumetric flow rate reduces the dwell time, which decreases the conversion efficiency of the catalysts [30]. Apart from this, the resulting exhaust gas composition due to the adapted engine calibration to altitude [15] also has an impact on the pollutants conversion. The O_2 partial pressure can be affected in parallel to the change in inhibition that is related to the CO and HC engine-out emission [31]. In fact, the same criteria for torque maximization applied to a variety of altitudes entail a CO increase to extreme high levels along with minimum O_2 availability, which can even cancel the catalytic activity [32].

In this work, the CO and HC conversion efficiencies in an oxidation catalyst were studied under steady state conditions running the engine at two different ambient conditions that were generated by the altitude simulator Horiba MEDAS (Multifunctional Efficient and Dynamic Altitude Simulator) [33,34]. The contour maps of the experimental conversion efficiencies were obtained at sea-level and 20 °C as the baseline condition and at 2500 m and −7 °C for the same exhaust mass flow and temperature ranges. The use of these common boundaries allowed for underlining the role of the dwell time and the partial pressure of the reactant species, which changed due to the ambient pressure and engine operation variation. The analysis of the experimental results was completed with the modeling of the catalyst in order to account for additional insights on the physical and chemical processes taking place in the monolithic reactor. In this regard, the CO and HC light-off curves were modeled to include progressively the effect of dwell time, O_2 partial pressure, and pollutants partial pressure on the conversion efficiency from warm sea-level to cold altitude operation.

2. Material and Methods

In this section, the main characteristics of the engine and the experimental setup are firstly provided. Next, the catalyst model thta was used in this study is briefly presented. Finally, the test and modeling procedure that was followed for determining the CO and HC conversion efficiencies as a function of the exhaust mass flow and catalyst inlet temperature is described in detail.

2.1. Experimental Setup

A HSDI diesel Euro 6d-Temp engine for passenger car applications was used to carry out this work. Table 2 summarizes the main characteristics of the engine. The engine

was equipped with variable geometry turbine (VGT) as well as HP- and cooled LP-EGR. The aftertreatment system was composed by a close-coupled diesel oxidation catalyst (DOC) and a wall-flow particulate filter coated as selective catalytic reduction system (SCRf) [35]. This study is focused on the DOC, whose main characteristics are listed in Table 3.

Table 2. Main specifications of the engine.

Engine type	HSDI diesel
Emissions Standards	Euro 6d-Temp
Number of cylinders	4 in line
Displaced volume [cm^3]	1461
Bore [mm]	76
Stroke [mm]	80.5
Number of valves	2 per cylinder
Compression ratio	15.2:1
Rated power @ speed	81 kW @ 4000 rpm
Rated torque @ speed	260 Nm @ 1750–2500 rpm
Fuel Injection	Common-rail direct injection
Turbocharger	VGT
EGR	HP- and cooled LP-EGR
ATS	Closed-coupled DOC + SCRf

Table 3. Main characteristics of the oxidation catalyst.

Substrate	Cordierite
Washcoat	Alumina oxide and β-zeolite
Coating	Pt
Monolith length [mm]	140
Monolith diameter [mm]	120
Channel cross-section	Square
Cell density [cpsi]	400
Cell size [mm]	1.04
Wall thickness [mm]	0.23
Catalytic area [m^2]	3.95

The engine was installed in a test bench that was equipped with an Elin EBG dynamometer controlled by AVL PUMA Open 2. According to the scheme that is shown in Figure 1, the most relevant characteristics of the experimental facility was the coupling of the engine with Horiba MEDAS, an altitude simulator that was developed by CMT-Motores Térmicos [33,34]. MEDAS provides variable working pressure to the engine as a function of the requested driving altitude. This simulator is coupled to the engine intake, exhaust, and sump, and it communicates with the engine control unit [36,37]. Additionally, the ambient temperature was imposed by means of the MEDAS temperature module (MTM), which was placed upstream of the MEDAS core module. With this setup, the driving conditions can be emulated in conventional test cells, with a variable altitude from sea-level to 5000 m and ambient temperature ranging between −15 and 45 °C.

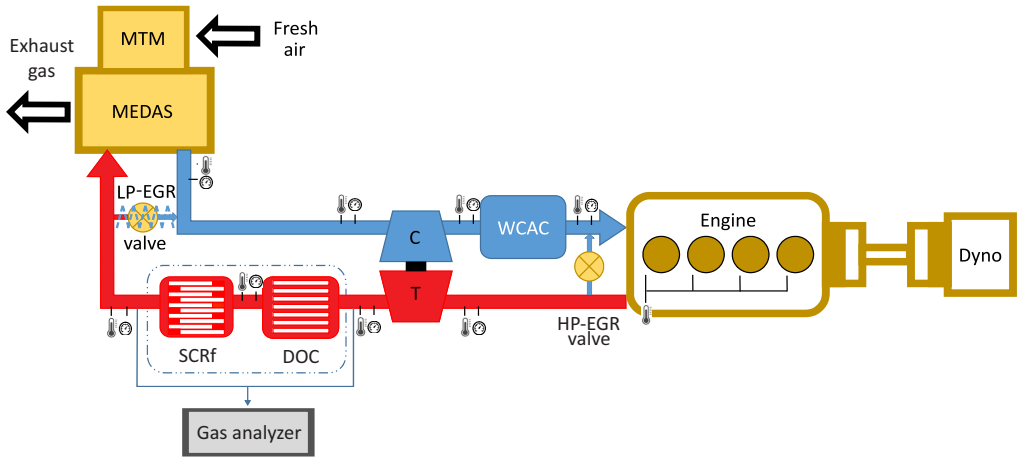

Figure 1. Scheme of the engine test bench.

The engine was fully instrumented to evaluate its performance and the abatement of CO and HC in the DOC. The engine speed and torque were set by the dynamometric brake. The air mass flow was obtained from the flow-meter that was monitored by engine control unit and accessed by ETAS INCA software. The fuel mass flow was measured with an AVL 733S gravimetric balance. The temperature and pressure were also measured along the flow path in the intake and exhaust lines while using K-type thermocouples and piezorresistive sensors, respectively. The exhaust gas composition was measured using Horiba Mexa-One gas analyzers, which sampled the exhaust gas upstream and downstream of the DOC in order to determine the CO and HC conversion efficiencies. A gas sample was also obtained at the intake manifold allowed for measuring the CO_2 concentration and determining the EGR rate. Only LP-EGR was used in this work.

2.2. Catalyst Model

A flow-through monolith model [38] comprising a reaction mechanism to deal with CO and HC abatement was employed in this work. The heat transfer was solved by means of a lumped nodal discretization [39], which considered gas to wall heat exchange as well as the heat that is released by the CO and HC oxidation, the heat losses toward the ambient and the effect of the thermal effect due to the ceramic substrate, the mat and the external canning. This way, the substrate temperature variation during every time-step was computed solving the general heat transfer equation by explicit centered finite differences as

$$\Delta T_w = \frac{\Delta t}{c_w}\left(\sum_i \frac{T_i - T_w}{r_i} + \dot{q}_r\right), \tag{1}$$

where Δt represents the time-step, T is the temperature, and r stands for the thermal equivalent resistance between i and the substrate. In these terms, the subscript i represents the gas or internal canning surface. The thermal inertia of the substrate was considered by means of the thermal capacitance (c_w). Finally, $\dot{q}_r$ represents the thermal power that is related to the reaction mechanism. This consisted of the CO and HC oxidation reactions in the presence of O_2, as well as the HC adsorption and desorption on the zeolite washcoat [40]:

$$CO + \frac{1}{2}O_2 \rightarrow CO_2 \tag{2}$$

$$C_nH_m + \left(n + \frac{m}{4}\right)O_2 \rightarrow nCO_2 + \frac{m}{2}H_2O \tag{3}$$

$$C_nH_m + \text{Zeolite} \rightleftarrows C_nH_m \cdot \text{Zeolite} \tag{4}$$

The HCs were represented by decane, as the most representative HC compound in diesel applications [41]. The CO and HC conversion efficiencies were determined solving

the one-dimensional chemical species transport assuming quasi-steady flow, flat velocity, and negligible concentration gradients in the washcoat [42], according to [25]:

$$u_{in}\frac{\partial p_n}{\partial x} = -S_{p,gas}k_{m,n}(p_n - p_{n,wc}) \tag{5}$$

$$\sum_i \nu_n R_i + S_{p,wc}k_{m,n}(p_n - p_{n,wc}) = 0 \tag{6}$$

Equation (5) represents the bulk gas transport, which involves the advective transport of species n along the monolith channels and its diffusion toward the washcoat interface. Although the use of the mole fraction to write the species conservation equations [25] is convenient in aftertreatment applications [42], the partial pressure (p_n) was considered in this work to make the impact of the gas pressure on the reaction rate explicit. In Equation (5), $S_{p,gas}$ represents the specific surface, which accounts for the catalytic surface to gas volume ratio, and k_m is the bulk mass transfer coefficient [43]. In a similar way, Equation (6) refers to the species n balance in the washcoat, with $S_{p,wc}$ being the washcoat specific surface, i.e., the inverse of the effective washcoat thickness [44] defined as the washcoat volume to catalytic surface ratio. The term R refers to the reaction rate, which is defined as a function of the reactants partial pressures for every reaction:

$$R_{ox,n} = \frac{k_{ox,n}}{G_{ox}}p_{O_2}p_{n,wc}, \quad \text{where n} = \text{CO, HC} \tag{7}$$

$$R_{ads,HC} = k_{ads,HC}(1 - \theta_{HC})\psi_{HC}p_{HC,wc} \tag{8}$$

$$R_{des,HC} = k_{des,HC}\theta_{HC}\psi_{HC} \tag{9}$$

In Equations (7)–(9), the kinetic constant k is defined according to the Arrhenius expression, θ and ψ represent the HC surface coverage and specific storage capacity, respectively, and G_{ox} is the inhibition term for CO and HC oxidation reactions, as proposed by Voltz et al. [45]:

$$G_{ox} = T_w(1 + K_1 p_{CO,wc} + K_2 p_{HC,wc})^2(1 + K_3 p_{CO,wc}^2 p_{HC,wc}^2)(1 + K_4 p_{NO,wc}^{0.7}) \tag{10}$$

2.3. Test and Modeling Procedure

The test campaign was conducted under steady state conditions to obtain the contour maps of the CO and HC conversion efficiencies as a function of the DOC gas inlet temperature and exhaust gas mass flow bounded by two different ambient conditions. Every test was carried out, keeping the engine under constant torque and speed [46], thus ensuring that the DOC boundary conditions were stable once thermal stabilization was reached. Firstly, the conversion efficiency of the pollutants was measured at sea-level and 20 °C, which will be referred as warm sea-level case and used as the baseline for comparison with the results at 2500 m, i.e., 0.747 bar in ambient pressure and −7 °C (cold altitude case). To do this, the engine speed was run at 1000 rpm, 1250 rpm, and 1500 rpm in warm sea-level, moving the speed range to higher values in cold altitude to cover similar exhaust mass flow in both cases. The gas temperature at the inlet of the catalyst was also controlled within the same range (100 to 300 °C) for both atmospheres by acting on the engine pedal. For every tested point, the measurement of the pollutants was carried out continuously following the measurement procedure that is sketched in Figure 2. The example represents the pedal position and the DOC inlet temperature for operating conditions at 1500 rpm and 200 °C in DOC inlet temperature for sea-level operation.

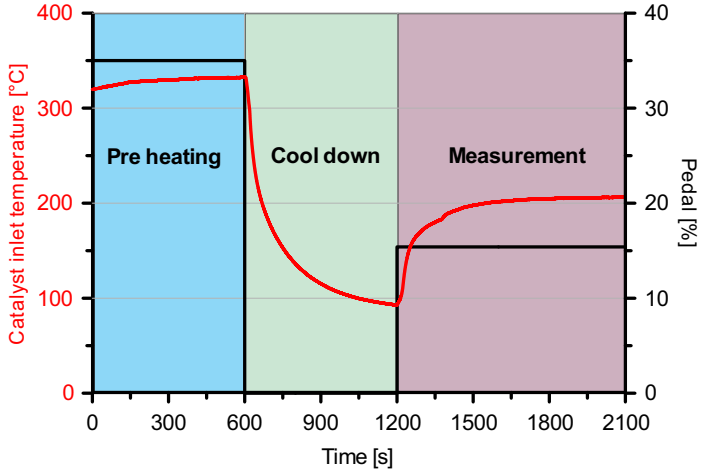

Figure 2. The test procedure for every steady state operating point considered to obtain the CO and HC conversion efficiency contour maps.

The procedure consisted of an initial preheating stage providing a DOC inlet temperature above 300 °C. This operating condition was maintained for 10 min. to ensure the desorption of all accumulated HC in the DOC due to previous tests [47]. Afterward, a cooling phase followed for another 10 min., during which the DOC inlet temperature converged to 100 °C. This way, all of the tests started at the same DOC state. Finally, the engine was run at the desired steady state conditions that aimed to complete the contour maps. The measurements were taken continuously during 15 min. to ensure the exhaust thermal stabilization.

The continuous measurement of emissions was required to identify the synergy between the oxidation and adsorption mechanisms on HC abatement. The adsorption is responsible for the high HC conversion efficiency at low temperature. In order to quantify the contribution of each HC abatement mechanism along the test, the modeling task consisted of the simulation of every steady state operating point along the entire test duration. Therefore, the calibration of the kinetic constants, which is summarized in Table 4, considered the influence of the thermal transient (effect on oxidation and adsorption-desorption equilibrium) along with the impact of the gradual HC accumulation (effect on adsorption–desorption reaction rate). This way, a steady state picture was taken at the end of the tests distinguishing HC oxidation and adsorption conversion efficiencies as a function of the ambient condition.

Table 4. Calibration of the reaction rate parameters.

Kinetic Constants		
	$\mathbf{P_f}$ [−]	$\mathbf{E_a}$ [J/mol]
HC adsorption	0.67	0
HC desorption	1×10^9	110,000
HC oxidation	1×10^{16}	85,000
CO oxidation	9×10^{15}	80,000
Inhibition Terms		
	$\mathbf{P_f}$ [−]	$\mathbf{E_a}$ [J/mol]
K_1	455	−7990
K_2	1×10^3	-3×10^3
K_3	2.98	−96,534
K_4	4.79×10^5	31,036

Figure 3 compares the experimental and modeling HC conversion efficiency from several operating points that were evaluated at warm sea-level and cold altitude. These

points cover low (100 °C) and high (250 °C) catalyst inlet temperature, so that the HC adsorption role can be identified.

Figure 3a represents the HC conversion efficiency along the test at 1000 rpm and 10 Nm (39 kg/h and 100 °C) for ambient conditions corresponding to warm sea-level. Complementary, Figure 3b provides the results at 1250 rpm and 3 Nm (42 kg/h and 100 °C) tested in cold altitude. Both of the operating conditions represent the minimum temperature region of the study, in which the adsorption processes of HC are more relevant, and low load engine operation, such as those occurring in transitory periods in RDE cycles [48] or in certain urban driving conditions [49].

As observed, all of the cases were modeled with good accuracy from initial conditions, with empty HC surface coverage, to the end of the test, once thermal stability was reached in the engine exhaust. The model was able to capture the progressive reduction of HC conversion efficiency along the test. The gradual increase of the HC surface coverage governed this decrease, which moved the equilibrium toward the desorption and decreased the adsorption contribution.

On the other hand, Figure 3c shows the HC conversion efficiency in the test at 1500 rpm and 50.5 Nm (75 kg/h and 250 °C) for warm sea-level conditions, whilst Figure 3d corresponds to 1500 rpm and 39.4 Nm (70 kg/h and 250 °C) at a cold altitude. At these higher mass flows and catalyst inlet temperatures, the conversion efficiency became constant over time after the thermal stabilization cut-off period, unlike what was shown for the low temperature tests. This is because the HC oxidation, which is the one that governs the chemical reaction in these tests, is independent of the state of the zeolite loading, but is only dependent on the temperature.

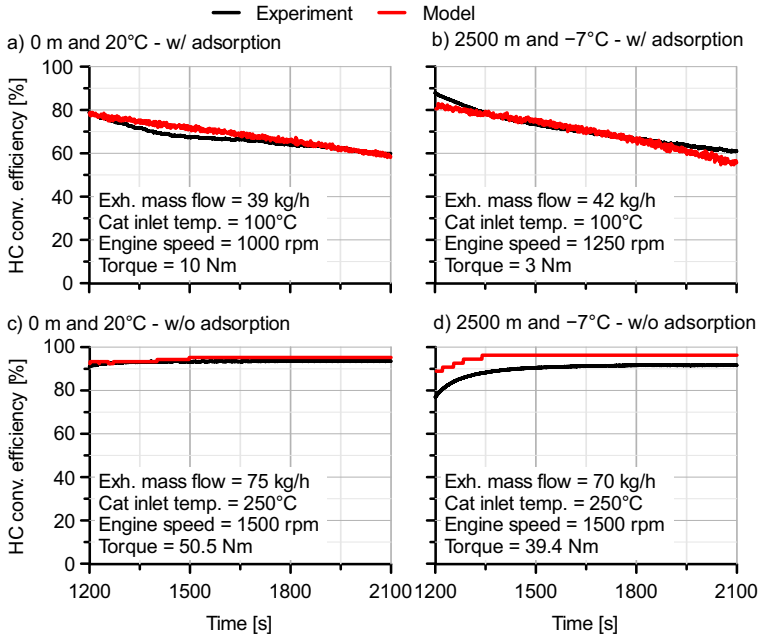

Figure 3. Comparison between experimental and modeled HC conversion efficiency during the tests at: (**a**) 0 m and 20 °C with 39 kg/h in exhaust mass flow and 100 °C in catalyst inlet temperature; (**b**) 2500 m and −7 °C with 42 kg/h in exhaust mass flow and 100 °C in DOC inlet temperature; (**c**) 0 m and 20 °C with 75 kg/h in exhaust mass flow and 250 °C in catalyst inlet temperature; and, (**d**) 2500 m and −7 °C with 70 kg/h in exhaust mass flow and 250 °C in DOC inlet temperature.

3. Discussion of the Results

This section is first devoted to the description of the experimental and modeled results concerning CO and HC conversion efficiencies. Next, the causes leading to the change in the conversion efficiency pattern from warm sea-level to cold altitude conditions are discussed.

3.1. CO and HC Conversion Efficiency

Figure 4 shows the CO conversion efficiency contour maps for the two tested ambient conditions as a function of the exhaust mass flow and DOC inlet temperature. The upper row represents the experimental (Figure 4a) and modeled (Figure 4b) CO conversion efficiency at sea-level and 20 °C, whilst Figure 4c,d do the same at 2500 m and −7 °C. The black dots on the contours represent the measured steady state points.

The comparison of Figure 4a,b reveals that the model was able to capture the trends in CO conversion efficiency in warm sea-level. The CO conversion efficiency was lower than 20% below 100 °C in the DOC inlet temperature, regardless the exhaust mass flow. However, as the DOC inlet temperature increased, the CO conversion efficiency and its sensitivity to the exhaust mass flow also did. The CO light-off showed a marked dependence on the exhaust mass flow, increasing from ∼120 °C at 40 kg/h to ∼150 °C at 68 kg/h, according to the experimental and modeled results. From this threshold, the light-off temperature showed even higher sensitivity to the mass flow. The model also accurately predicted the region reaching 100% of CO conversion efficiency. Again, the maximum conversion efficiency was reached earlier for minimum mass flow, increasing slowly from ∼160 °C in DOC inlet temperature at 40 kg/h to ∼210 °C at 71 kg/h. In this temperature range, a further increase of the exhaust mass flow at constant temperature also led to a faster deterioration of the CO conversion efficiency.

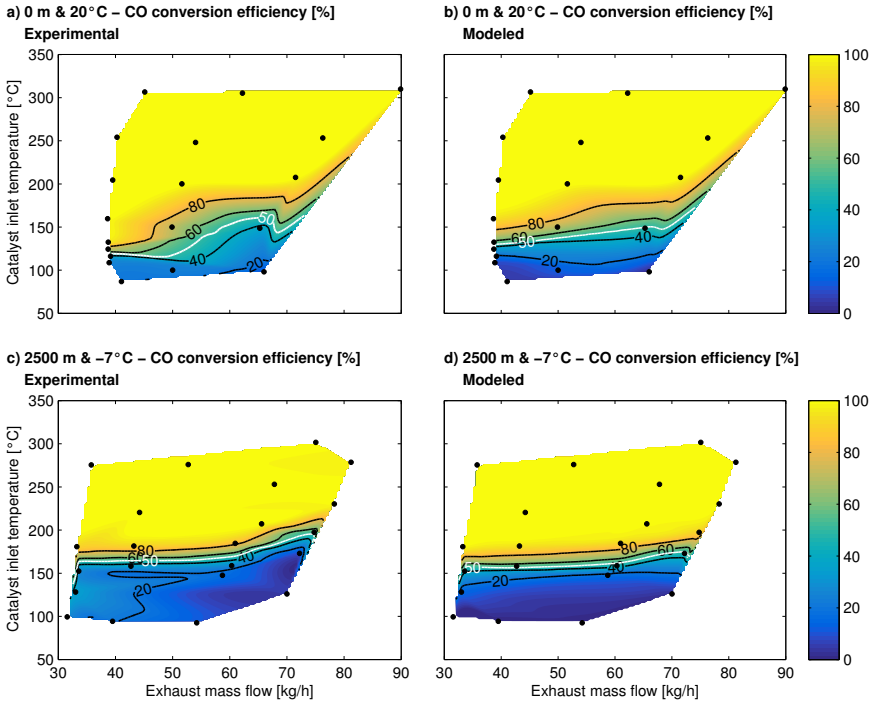

Figure 4. CO conversion efficiency as a function of the exhaust mass flow and catalyst inlet temperature: (**a**) experimental results at 0 m and 20 °C; (**b**) modeled results at 0 m and 20 °C; (**c**) experimental results at 2500 m and −7 °C; and, (**d**) modeled results at 2500 m and −7 °C.

When comparing warm sea-level results with those corresponding to cold altitude (Figure 4c), which were also reproduced with high accuracy by the model (Figure 4d), the change in CO conversion efficiency fashion is evidenced. For these extreme ambient conditions, the CO light-off temperature was delayed until ∼165 °C at 40 kg/h and remained almost constant until 60 kg/h. This involves an increase of light-off temperature ranging between 45 and 15 °C with respect to the warm sea-level. The complete CO abatement was also reached at higher temperatures, which varied linearly from ∼190 °C to ∼230 °C between 40 kg/h and 78 kg/h. The deterioration of the CO conversion efficiency in cold altitude was extensible to the entire exhaust mass flow range, although it was more penalized at low exhaust mass flows.

Figure 5 presents the experimental and modeled contour maps of the HC conversion efficiency at each ambient condition in the same manner. An overview of the results confirms that the model was also accurate regarding HC abatement prediction, with high sensitivity to the exhaust mass flow and DOC inlet temperature for both ambient conditions.

Cold altitude conditions also moved down the HC conversion efficiency, although with different trends to the CO case. The adsorption on the zeolites provided the HC with higher conversion efficiencies at low temperature than those that were found for CO. In warm sea-level, the HC conversion efficiency was over 60% and reached 80% at ∼170 °C. This temperature was kept almost constant until 70 kg/h, from which a decrease of the HC conversion efficiency started, as also found in CO case. The model provided similar fashion of the results, although with a slightly conversion efficiency variation with the exhaust mass flow. Above 170 °C in DOC inlet temperature, the HC conversion efficiency increased very slowly and it was only greater than 90% for temperatures that were above ∼250 °C.

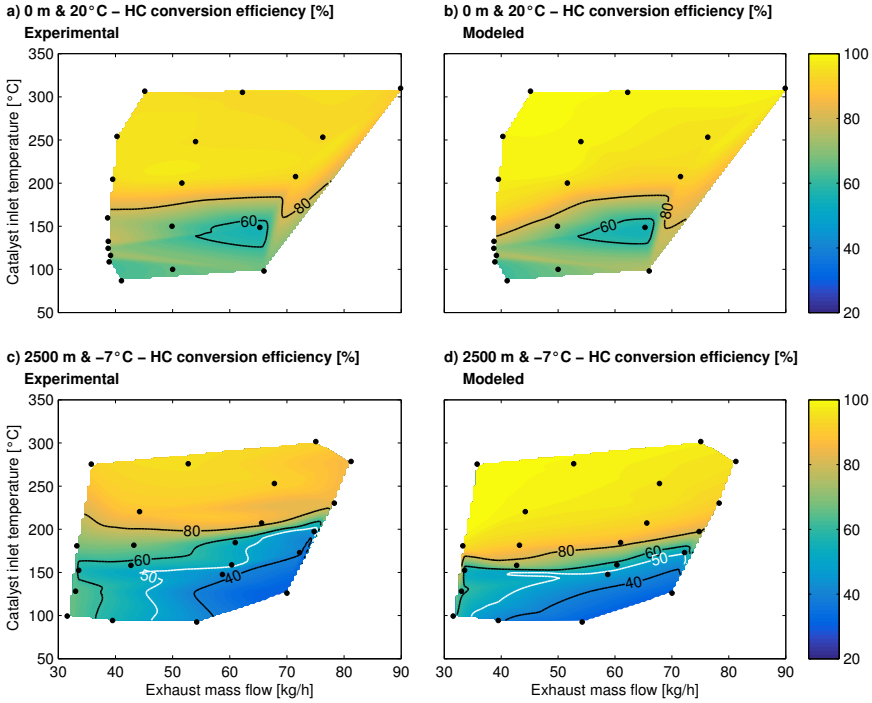

Figure 5. HC conversion efficiency as a function of the exhaust mass flow and catalyst inlet temperature: (**a**) experimental results at 0 m and 20 °C; (**b**) modeled results at 0 m and 20 °C; (**c**) experimental results at 2500 m and −7 °C; and, (**d**) modeled results at 2500 m and −7 °C.

The HC was not completely depleted in the tested DOC inlet temperature window, which was most probably due to the existence of very low reactivity HC species [50]. This result was similar for warm sea-level and cold altitude at high temperature. However, higher DOC inlet temperature was required to reach the same conversion efficiency in cold altitude. As example, 200 °C were required to reach 80% of HC conversion efficiency in cold altitude, i.e., 30 °C above the conditions in warm sea-level. In fact, the HC conversion efficiency in cold altitude fell fast below this temperature, with a clear dependence on the exhaust mass flow. Whilst the HC conversion efficiency remained around 60% between and 100–150 °C at a low exhaust mass flow, it sharply decreased as the mass flow increased, reaching 30% at 70 kg/h and 125 °C.

The phenomena leading to the decrease of the conversion efficiency are common for CO and HC, as later discussed in Section 3.2. However, as previously stated, the CO and HC conversion efficiency patterns were different because of the HC adsorption. This was contrasted computing the HC conversion efficiencies due to adsorption and oxidation phenomena separately. Figure 6 represents these contributions as a function of the exhaust

mass flow and the DOC inlet temperature. Plots (a) and (b) in Figure 6 are related to the HC oxidation conversion efficiency in warm sea-level and cold altitude, respectively. Complementary, plots (c) and (d) in Figure 6 show the adsorption contribution. As observed, the trends in Figure 6a,b, i.e., HC oxidation, were exactly the same as those that were obtained for CO conversion efficiency (comparison with Figure 4) at each tested atmosphere.

Table 5 numerically exemplifies the trends in conversion efficiency. The CO and HC conversion efficiency are considered. In the case of HC, the oxidation and adsorption contributions to the total HC conversion efficiency are distinguished. The CO and HC oxidation conversion efficiency increase with the DOC inlet temperature, while the HC adsorption conversion efficiency shows decreasing values. Because the same expressions govern the oxidation reaction rate for CO and HC, the quantitative differences come mostly from the lower HC reactivity and the CO/HC partial pressures to a lesser extent, as forward discussed. Therefore, the adsorption was indeed the main source of discrepancy between CO and HC conversion efficiencies. Noting that the results correspond to the conditions after 15 min. of operation (the adsorption is a time-governed process), the HC adsorption conversion efficiency in warm sea-level was ∼60% until ∼125 °C (point B in Table 5), regardless of the mass flow and it dropping quickly as the DOC inlet temperature increased (∼20% at ∼150 °C). Equivalently, Table 5 shows how the adsorption conversion efficiency drops by increasing the DOC inlet temperature. In cold altitude, these orders of magnitude were only obtained at very low mass flow (Figure 6d and point F in Table 5). In these conditions, the adsorption HC conversion efficiency was highly penalized as the mass flow increased, in contrast to the warm sea-level (Figure 6c). The adsorption-desorption equilibrium is determined by the HC partial pressure and the HC surface coverage evolution over time, according to Equations (8) and (9). Section 3.2 discusses their impact on the resulting adsorption HC conversion efficiency.

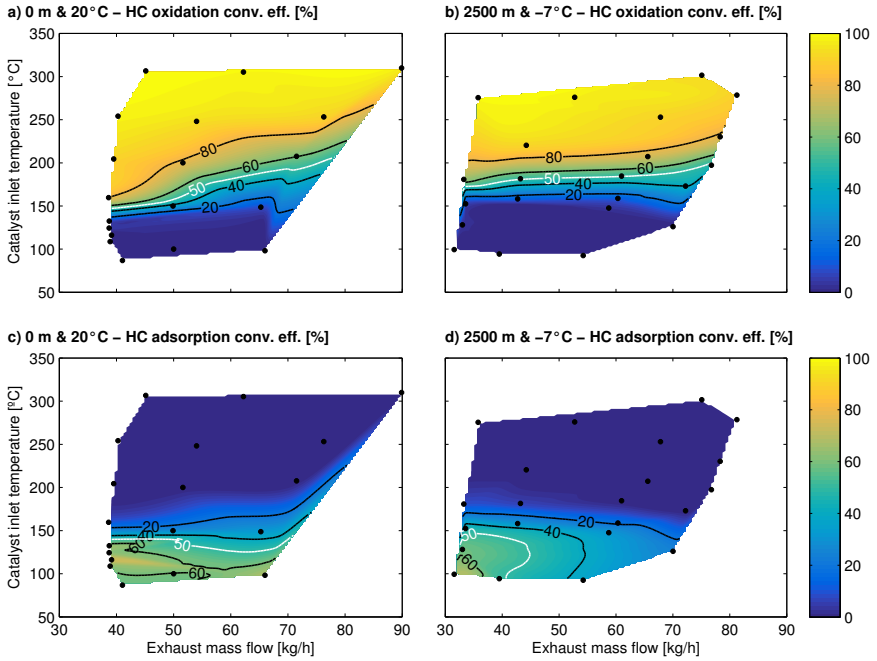

Figure 6. Adsorption and oxidation contributions to HC conversion efficiency as a function of the exhaust mass flow and catalyst inlet temperature: (**a**) oxidation at 0 m and 20 °C; (**b**) oxidation at 2500 m and −7 °C; (**c**) adsorption at 0 m and 20 °C; and, (**d**) adsorption at 2500 m and −7 °C.

3.2. Role of Flow Properties in Conversion Efficiency Variation

The DOC inlet temperature and exhaust mass flow are engine parameters that are intimately related to the air and thermal management. In addition, the results that are presented in Section 3.1 have shown that they have a relevant impact on the pollutants

Table 5. Oxidation and adsorption conversion efficiencies at selected points.

Point	Condition	Temp. [°C]	Mass Flow [kg/h]	CO eff. [%]	HC ox. eff. [%]	HC ads. eff. [%]	Total HC eff. [%]
A	0 m & 20 °C	98.17	66.00	1.09	0.00	68.83	68.83
B	0 m & 20 °C	124.40	38.72	32.25	5.22	62.60	67.82
C	0 m & 20 °C	159.61	38.64	93.89	79.44	11.35	90.79
D	0 m & 20 °C	253.22	76.29	100.00	89.52	0.00	89.52
E	2500 m & −7 °C	92.53	54.22	0.17	0.00	37.41	37.41
F	2500 m & −7 °C	128.13	33.02	14.64	3.45	58.62	62.07
G	2500 m & −7 °C	158.78	60.33	44.27	12.35	18.52	30.87
H	2500 m & −7 °C	230.25	78.31	99.19	78.33	0.00	78.33

abatement. However, since the tested ranges are equivalent for warm sea-level and cold high altitude cases, the underlying causes explaining the change in conversion efficient must be found in additional parameters, namely dwell time and reactants partial pressure.

Figure 7 represents the dwell time as a function of the exhaust mass flow and DOC inlet temperature for the tested ambient conditions. The dwell time is evidently lower when working in altitude conditions for the same exhaust mass flow and DOC inlet temperature, as expected from the lower exhaust pressure after the VGT expansion in altitude operation. In this particular study, the altitude dwell time was decreased by a ∼25% with respect to sea-level, according to the ambient pressure reduction from sea-level to 2500 m. Consequently, this parameter is negatively affecting the conversion efficiency in the cold altitude case in an homogeneous way throughout the tested range.

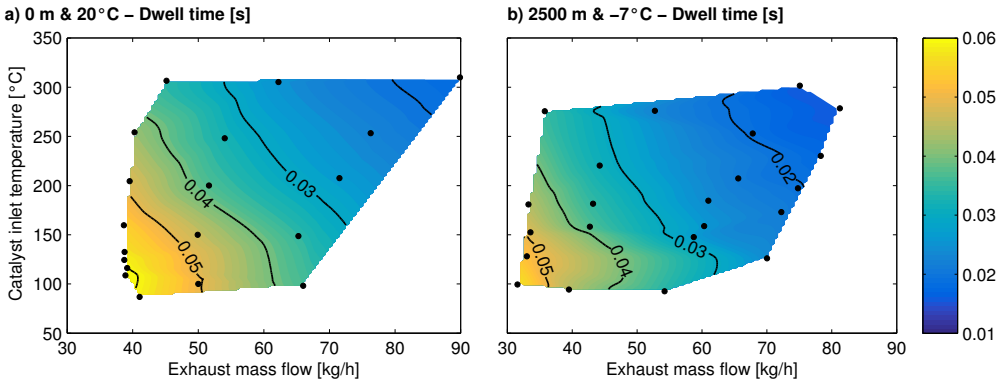

Figure 7. Dwell time as a function of the exhaust mass flow and catalyst inlet temperature: (**a**) 0 m and 20 °C; (**b**) 2500 m and −7 °C.

Opposite to dwell time, the reactants partial pressures can differently affect as a function of the exhaust mass flow and DOC inlet temperature because of their relation with the engine operating point. Partial pressure provides dual sensitivity because of the exhaust pressure at the VGT outlet, which is mostly given by the altitude, and the mole fraction, which is determined by the engine management as a function of both altitude and ambient temperature.

Figure 8 plots the O_2 partial pressure. At very low temperature, the O_2 partial pressure was lower in cold altitude than in the warm sea-level. This was expected from the lower ambient pressure in altitude conditions. As a consequence, it contributed to lower CO and HC reactivity in the oxidation light-off and warm-up regions during altitude operation. This result is in agreement with the trends in conversion efficiency that are described in Section 3.1. If the ratio of O_2 partial pressures between altitudes was exclusively related to ambient pressure variation, its ratio should be 1.356 (sea-level to 2500 m ambient pressure ratio) in the entire contour map. However, this ratio was lower everywhere and variable with exhaust mass flow at constant DOC inlet temperature. At very low temperature,

the O_2 partial pressure at sea-level was very sensitive to the exhaust mass flow, although higher than at altitude; at high temperatures, the O_2 partial pressures at sea-level and altitude tended to converge. In fact, the O_2 partial pressure resulted in being lower at sea-level above 250 °C for low exhaust mass flows than in the altitude counterpart.

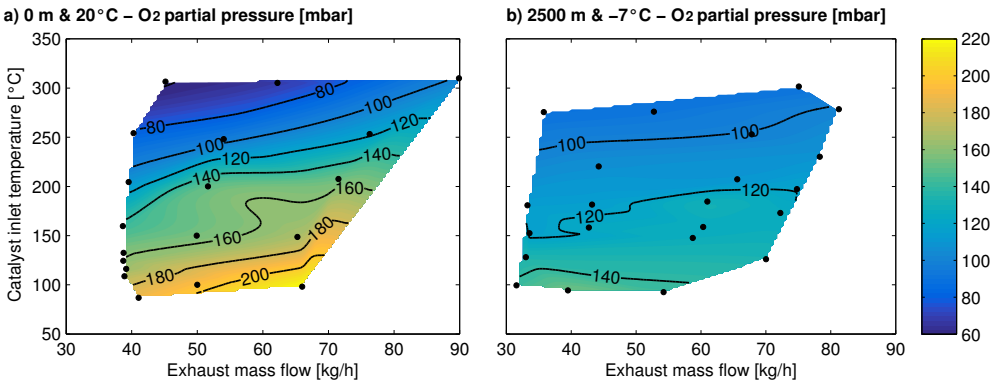

Figure 8. O_2 partial pressure as a function of the exhaust mass flow and catalyst inlet temperature: (**a**) 0 m and 20 °C; (**b**) 2500 m and −7 °C.

These trends evidence that additional engine variables conditioned the DOC performance. Figure 9 represents the fields of equivalence ratio and LP-EGR rate in the tested conditions. According to plots (a) and (b) shown in Figure 9, the equivalence ratio was higher for warm sea-level in the entire tested range, but especially at high DOC inlet temperature. Comparatively, it contributed to offsetting the expected differences in O_2 partial pressure due to altitude operation. The increasing O_2 partial pressure with exhaust mass flow at constant DOC inlet temperature corresponding to warm sea-level (Figure 8) was also dictated by the inverse trend in equivalence ratio. As a remark, the operation in cold altitude required higher engine speed and fuel mass flow, besides higher boost pressure (closer VGT, and higher turbine inlet pressure and temperature), for the same exhaust mass flow and DOC inlet temperature. In addition, the differences in the equivalence ratio were also influenced by the huge variation in LP-EGR rate between the sea-level and altitude cases. The engine control closed the LP-EGR valve, which, besides the increase of the boost pressure, offset the air mass flow reduction with respect to sea-level driving [12] and contributed to setting an adequate equivalence ratio [13]. Figure 9c,d show that the fields of LP-EGR are equivalent in trend in warm sea-level and cold altitude. The LP-EGR rate increases with the exhaust mass flow (engine speed), but the increasing rate is lower as the mass flow increases. It also contributes to explaining the lower equivalence ratio and higher O_2 partial pressure at high exhaust mass flow.

Regarding the CO conversion efficiency, Figure 10 represents the engine-out CO partial pressure for the two tested ambient conditions. A change in the sensitivity of the CO partial pressure with exhaust mass flow and catalyst inlet temperature is observed between the warm sea-level and cold altitude cases. In the warm sea-level condition, the CO partial pressure was highly dependent on the temperature at low exhaust mass flow. However, the CO emission became increasing as the exhaust mass flow did. By contrast, the CO partial pressure was mostly dependent on the DOC inlet temperature in cold altitude operation. It is very interesting to note that, despite the lower ambient pressure, the highest CO partial pressure was found in these conditions at a low DOC inlet temperature.

When considering the engine-out HC partial pressure, which is represented in Figure 11, the trends are very similar to those that are found for CO. Again, the maximum HC partial pressure took place at low DOC inlet temperature in the case of altitude operation. The fact that the CO and HC partial pressures were higher in a cold altitude than the warm sea-level counterparts evidenced higher engine-out emission (mole fraction). This trend covers the entire engine-out HC field but only the medium-low DOC inlet temperature range for CO. In the case of HC, it is also remarkable that the high engine-out

HC emission at low temperature determined the adsorption efficiency along time. Higher HC emission at altitude conditions meant higher HC adsorption conversion efficiency at the beginning of the test. However, the faster increase of the HC surface coverage as time went by made the desorption rate increase. This is the reason why the HC adsorption conversion efficiency was lower in cold altitude than in warm sea-level at the end of the tests (Figure 6c,d), especially as the exhaust mass flow increased, since it caused greater HC surface coverage.

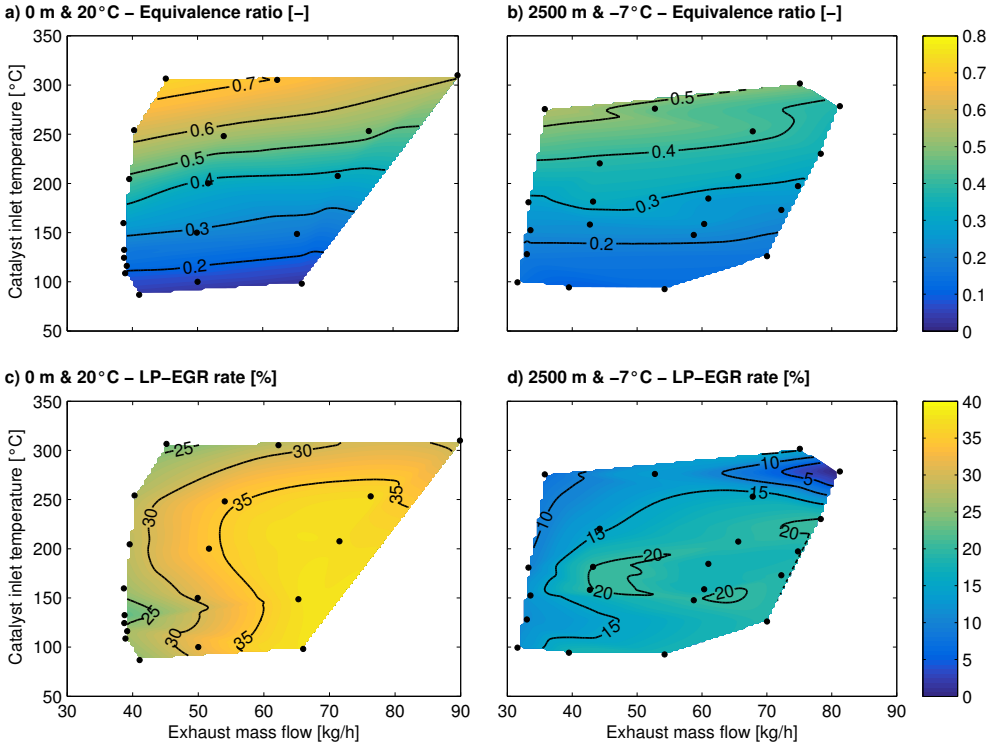

Figure 9. Equivalence ratio and low-pressure-exhaust gas recirculation (LP-EGR) rate as a function of the exhaust mass flow and catalyst inlet temperature: (**a**) equivalence ratio at 0 m and 20 °C; (**b**) equivalence ratio at 2500 m and −7 °C; (**c**) LP-EGR rate at 0 m and 20 °C; and, (**d**) LP-EGR rate at 2500 m and −7 °C.

Regarding a first-order reaction kinetic term, high CO/HC partial pressures at low temperature in altitude operation should contribute to offset the decrease in conversion efficiency caused by the lower dwell time and O_2 partial pressure. However, a high partial pressure of pollutant species also produces a penalty in inhibition [25]. Figure 12 depicts the oxidation inhibition term for two tested exhaust mass flows as a function of the DOC inlet temperature and ambient condition. The high CO and HC partial pressures at low temperature caused high inhibition in the cold altitude conditions. In both of the tested cases, the inhibition decreased as the temperature was increased because of the reduction in CO and HC partial pressures. The reduction of the engine-out emission combined with the lower ambient pressure gave, as a result, even lower inhibition than at sea-level. Therefore, the trends in partial pressures at low temperature (lower O_2, and higher CO and HC partial pressures in altitude) explain the decrease of the CO and HC conversion efficiency at high altitude, along with the dwell time decrease. Complementary, the DOC performance at high temperature was only damaged by the dwell time, with its penalty being reduced by the lower inhibition and the null influence of O_2. Hence, CO and HC conversion efficiencies resulted in being very similarly above ∼170 °C, regardless of the ambient condition.

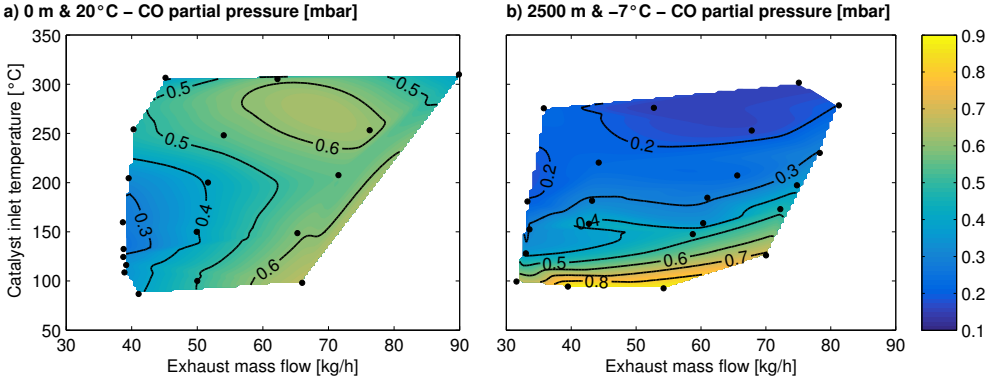

Figure 10. Engine-out CO partial pressure as a function of the exhaust mass flow and catalyst inlet temperature: (**a**) 0 m and 20 °C; (**b**) 2500 m and −7 °C.

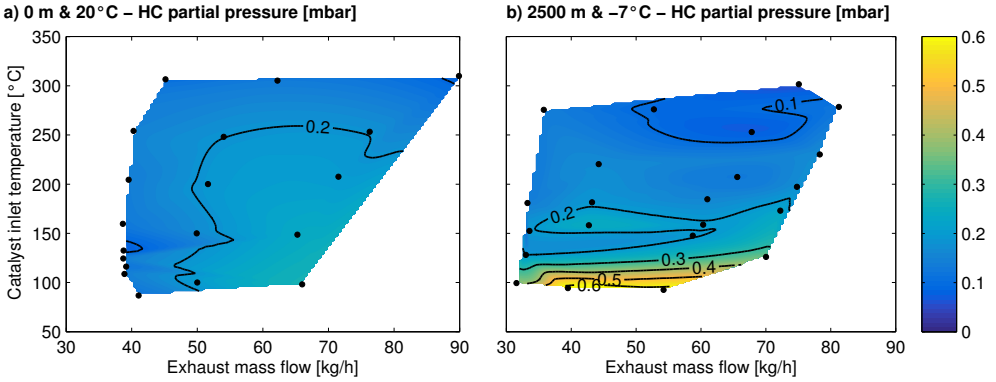

Figure 11. Engine-out HC partial pressure as a function of the exhaust mass flow and catalyst inlet temperature: (**a**) 0 m and 20 °C; (b) 2500 m and −7 °C.

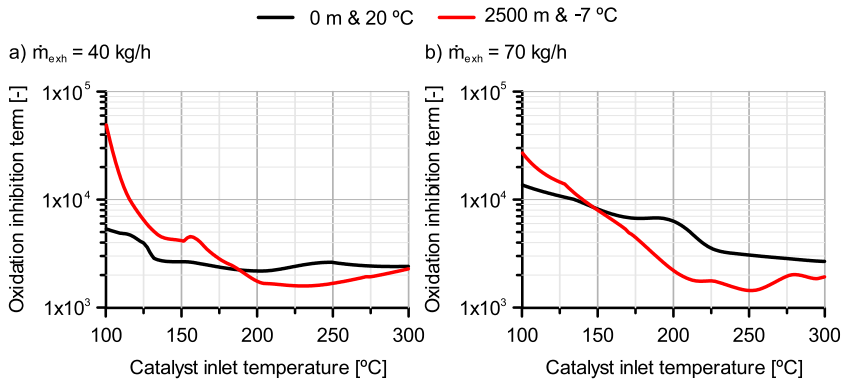

Figure 12. Inhibition term as a function of the DOC inlet temperature and ambient conditions for (**a**) 40 kg/h and (**b**) 70 kg/h in exhaust mass flow.

3.3. Light-Off Curves Sensitivity Analysis

Light-off curves of CO and HC were computed in order to evaluate the impact of the dwell time and the reactants partial pressure on the conversion efficiency separately. A set of light-off simulations were carried out for two exhaust mass flows (40 and 70 kg/h), imposing a DOC inlet temperature ramp of 1 °C/min from 100 °C to 300 °C. This small temperature ramp makes the efficiencies shown in the light-off curve equivalent to those that would be obtained when the catalyst operates under steady state conditions at every temperature. The gas composition was taken from the contour maps for every reactant.

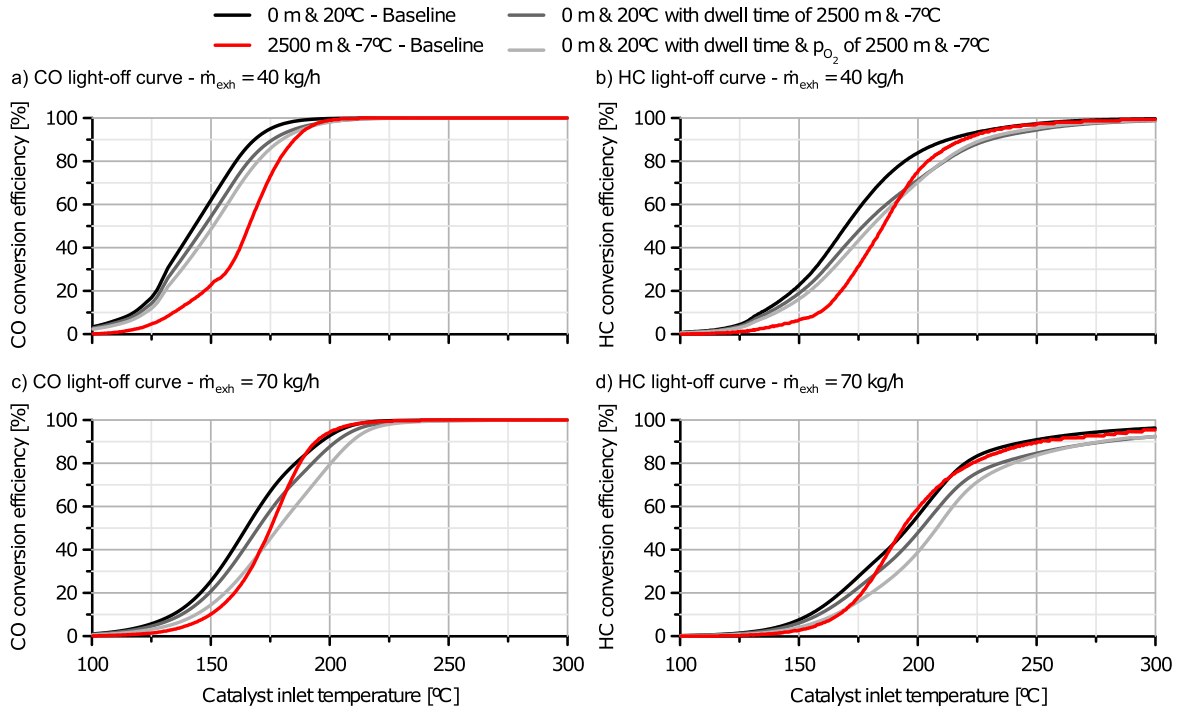

Figure 13. Progressive CO and HC light-off curves variation from warm sea-level to cold altitude case considering dwell time and reactants partial pressure separately: (**a**) CO light-off curve at 40 kg/h; (**b**) HC light-off curve at 40 kg/h; (**c**) CO light-off curve at 70 kg/h; and, (**d**) HC light-off curve at 70 kg/h.

Figure 13 represents the CO and HC light-off curves. In the case of HC, the adsorption mechanism was canceled, since it depends not only on temperature, but also time through the instantaneous surface coverage. Therefore, only the HC oxidation light-off curve was computed. Figure 13a,b represent the CO and HC light-off curves, respectively, corresponding to 40 kg/h, whilst plots (c) and (d) correspond to 70 kg/h. Four modeled series are compared in every plot to analyze, step-by-step, the change in conversion efficiency from warm sea-level to cold altitude conditions:

- The black series corresponds to the baseline warm sea-level case, i.e., experimental dwell time and gas composition at 0 m and 20 °C.
- As a first step, the dark gray series represents the results of a simulation where the warm sea-level setup was modified, imposing the dwell time that corresponds to cold altitude.
- Next, the light gray series was obtained from warm sea-level case, but imposing both the dwell time and O_2 partial pressure of the cold altitude case.
- Finally, the red series corresponds to the baseline cold altitude, i.e., dwell time, O_2 partial pressure, and pollutants partial pressure (kinetic term and inhibition) impact with respect to warm sea-level results.

As a common trend in every plot of Figure 13, the decrease of dwell time in altitude conditions produced a shift of the light-off curves toward higher temperatures (∼5.5 °C, on average). The decrease of the O_2 partial pressure also shifted the curves toward higher temperature in the light-off region. In this case, the penalty depended on the engine operating conditions, due to the variation of the O_2 partial pressure difference between warm sea-level and cold altitude as a function of the exhaust mass flow. The light-off temperature was further delayed ∼4.5 °C at 40 kg/h increasing the penalty until ∼7 °C at 70 kg/h. Nevertheless, the higher O_2 partial pressure at high temperature in cold altitude canceled its negative impact and slightly increased the HC conversion efficiency above ∼225 °C, as observed in Figure 13b.

Despite the deterioration of the light-off temperature due to dwell time and O_2 contributions in cold altitude, the red series evidenced that the most relevant parameters are the pollutants partial pressures due to the inhibition effect. At low exhaust mass flow (40 kg/h) and DOC inlet temperature, the CO and HC light-off curves were moved toward very high temperature, given rise to a substantial delay of the light-off temperature. It was more marked in the CO case (Figure 13a) due to its baseline low light-off temperature, which corresponds to an operating region where the CO and HC partial pressures were much more higher in the cold altitude than warm sea-level conditions. By contrast, the CO and HC partial pressures at a high temperature were lower in cold altitude than in warm sea-level. Consequently, the HC conversion efficiency improved with respect to the warm sea-level case above 200 °C, offsetting both the dwell time and O_2 partial pressure penalties. This result was not observed for CO in the 40 kg/h case due to the fact that its conversion efficiency was almost 100% at this temperature range.

As the mass flow increased (70 kg/h), the CO and HC partial pressures in cold altitude were only higher than in warm sea-level for a very low temperature, but rapidly decreased below the baseline condition. As a result, the light-off curves underwent a very fast increase of their slope in the cold altitude case (Figure 13c,d). The resulting CO light-off temperature was not further damaged and partially compensated the dwell time and O_2 partial pressure effects. Above this temperature, the benefits of the lower pollutants partial pressure became more evident and the light-off curves of the two tested ambient cases were even coincident from 185 °C on. The HC light-off benefited more from these boundary conditions, taking place earlier in cold altitude than in warm sea-level. In any case, both of the light-off curves converged from 50% in conversion efficiency.

4. Summary and Conclusions

This study has presented the trends of the CO and HC conversion efficiency variation in an oxidation catalyst, due to the change of the ambient conditions from standard warm sea-level to extreme operation in cold altitude (2500 m and −7 °C). The evaluation of the catalyst performance was carried out in a Euro 6d-Temp diesel engine run under steady-state conditions within a common range of exhaust mass flow and catalyst inlet temperature in both ambient conditions.

The CO and HC conversion efficiencies were deteriorated at low temperature, increasing the light-off temperature, but with different trends in CO and HC. The CO conversion efficiency suffered a very marked decrease in the low exhaust mass flow region, where the light-off was delayed approximately 45 °C. This penalty progressively decreased as the exhaust mass flow increased. The HC abatement was more damaged. Being the HC conversion efficiency above 50% in the entire tested field for warm sea-level, very low conversion efficiency regions were found in cold altitude operation, specially at high mass flow. In this case, the HC light-off was not reached until 150 °C from 50 kg/h onward in exhaust mass flow. The modeling of the DOC response revealed that the differences that were found in the variation of the CO and HC conversion efficiencies were exclusively due to the role of the adsorption process. This was highly influenced by the change in HC emission at a low temperature. The HC partial pressure in cold altitude became much higher than the one in warm sea-level, despite the lower ambient pressure. Consequently, the adsorption was very high at the beginning of the test. However, once the engine reached the steady-state conditions, the high HC surface coverage penalized the HC conversion efficiency in the low temperature region.

Concerning the causes of the oxidation light-off temperature variation, the dwell time and O_2 partial pressure were noticed to have a relevant influence in increasing it for both HC and CO in cold altitude operation. While the dwell time is unavoidable, the O_2 partial pressure depends on the exhaust temperature mainly due to its relation with the equivalence ratio. These parameters only damaged altitude operation at very low temperature, adding its negative contribution to the light-off temperature increase. However, the pollutants partial pressure were particularly critical in understanding the

deterioration of the conversion efficiency at low temperature. The reason was the huge increase of pollutant engine-out emission in altitude operation in this range of working conditions. Consequently, a high increase of the CO and HC oxidation inhibition was produced, thus highlighting the importance of an optimal engine control and ATS matching.

Author Contributions: Conceptualization, J.R.S. and P.P.; Formal analysis, P.P. and E.J.S.; Funding acquisition, J.R.S.; Investigation, J.R.S., P.P., E.J.S. and B.D.; Methodology, P.P. and B.D.; Project administration, J.R.S. and P.P.; Resources, J.R.S.; Software, P.P. and E.J.S.; Supervision, J.R.S. and P.P.; Visualization, E.J.S. and B.D.; Writing—original draft, P.P., E.J.S. and B.D.; Writing—review and editing, J.R.S., P.P., E.J.S. and B.D. All authors have read and agreed to the published version of the manuscript.

Funding: This research has been partially supported by FEDER and the Government of Spain through project TRA2016-79185-R. Additionally, the PhD candidate Bárbara Diesel has been funded by a grant from the Government of Generalitat Valenciana and FSE (European Union) with reference ACIF/2018/109.

Conflicts of Interest: The authors declare no conflict of interest.

Abbreviations

The following abbreviations are used in this manuscript:

Acronyms

ATS	aftertreatment system
DOC	diesel oxidation catalyst
EGR	exhaust gas recirculation
HP-EGR	high pressure EGR
HSDI	high-speed direct injection
LP-EGR	low pressure EGR
MEDAS	multifunctional efficient dynamic altitude simulator
MTM	MEDAS temperature module
RDE	real driving emission
SCRf	wall-flow particulate filter with selective catalytic reduction function
VGT	variable geometry turbine
WCAC	water charge air cooler
WLTC	worldwide harmonized light vehicle test cycle
WLTP	worldwide harmonized light vehicle test procedure

Latin Letters

c_w	thermal capacitance
D	monolith diameter
E_a	activation energy
G_{ox}	oxidation inhibition term
k_m	mass transfer coefficient
k_r	kinetic constant in reaction r
K	inhibition term constant
L	monolith length
$\dot{m}_{exh}$	exhaust mass flow
p_n	partial pressure of species n
P_f	pre-exponential factor
$\dot{q}_r$	thermal power related to the reaction mechanism
r	equivalent thermal resistance
R	reaction rate
S_p	specific surface
t	time
T	temperature
u	gas velocity
x	axial coordinate

Greek letters	
Δ	variation
ν	stoichiometric coefficient
θ	HC surface coverage
ψ	specific storage capacity
Subscripts	
ads	adsorption
des	desorption
gas	exhaust gas
in	inlet
n	species *n*
ox	oxidation
w	wall
wc	washcoat

References

1. Serrano, J.R.; Novella, R.; Piqueras, P. Why the development of internal combustion engines is still necessary to fight against global climate change from the perspective of transportation. *Appl. Sci.* **2019**, *9*, 4597. [CrossRef]
2. Joshi, A. Review of Vehicle Engine Efficiency and Emissions. SAE Technical Paper 2020-01-0352. 2020. Available online: https://www.sae.org/publications/technical-papers/content/2020-01-0352/ (accessed on 23 December 2020).
3. Commission Regulation (EU) 2017/1151 of 1 June 2017 Supplementing Regulation (EC) No 715/2007 of the European Parliament and of the Council on Type-Approval of Motor Vehicles with Respect to Emissions from Light Passenger and Commercial Vehicles (Euro 5 and Euro 6) and on Access to Vehicle Repair and Maintenance Information, Amending Directive 2007/46/EC of the European Parliament and of the Council, Commission Regulation (EC) No 692/2008 and Commission Regulation (EU) No 1230/2012 and Repealing Commission Regulation (EC) No 692/2008. Available online: https://eur-lex.europa.eu/legal-content/EN/TXT/?uri=CELEX%3A32017R1151 (accesed on 23 December 2020).
4. UNEP—World Conservation Monitoring Centre. The Delineation of European Mountain Areas. 2000. Available online: https://ec.europa.eu/regional_policy/sources/docgener/studies/pdf/montagne/mount4.pdf (accessed on 14 December 2020).
5. Serrano, J.R.; Piqueras, P.; Abbad, A.; Tabet, R.; Bender, S.; Gómez, J. Impact on reduction of pollutant emissions from passenger cars when replacing Euro 4 with Euro 6d diesel engines considering the altitude influence. *Energies* **2019**, *12*, 1278. [CrossRef]
6. Luján, J.M.; Climent, H.; García-Cuevas, L.M.; Moratal, A. Pollutant emissions and diesel oxidation catalyst performance at low ambient temperatures in transient load conditions. *Appl. Therm. Eng.* **2018**, *123*, 1527–1537. [CrossRef]
7. Ko, J.; Jin, D.; Jang, W.; Myung, C.L.; Kwon, S.; Park, S. Comparative investigation of NOx emission characteristics from a Euro 6-compliant diesel passenger car over the NEDC and WLTC at various ambient temperatures. *Appl. Energy* **2018**, *187*, 652–662. [CrossRef]
8. Luján, J.M.; Climent, H.; Ruiz, S.; Moratal, A. Influence of ambient temperature on diesel engine raw pollutants and fuel consumption in different driving cycles. *Int. J. Engine Res.* **2019**, *20*, 877–888. [CrossRef]
9. Lapuerta, M.; Ramos, Á.; Fernández-Rodríguez, D.; González-García, I. High-pressure versus low-pressure exhaust gas recirculation in a Euro 6 diesel engine with lean-NOx trap: Effectiveness to reduce NOx emissions. *Int. J. Engine Res.* **2019**, *20*, 155–163. [CrossRef]
10. Galindo, J.; Navarro, R.; Tarí, D.; Moya, F. Development of an experimental test bench and a psychrometric model for assessing condensation on a low-pressure exhaust gas recirculation cooler. *Int. J. Engine Res.* **2020**. [CrossRef]
11. Szedlmayer, M.; Kweon, C. Effect of Altitude Conditions on Combustion and Performance of a Multi-Cylinder Turbocharged Direct Injection Diesel Engine. SAE Technical Paper 2016-01-0742. 2016. Available online: https://www.sae.org/publications/technical-papers/content/2016-01-0742/ (accessed on 23 December 2020).
12. Bermúdez, V.; Serrano, J.R.; Piqueras, P.; Gómez, J.; Bender, S. Analysis of the role of altitude on diesel engine performance and emissions using an atmosphere simulator. *Int. J. Engine Res.* **2017**, *18*, 105–117. [CrossRef]
13. Ramos, A.; García-Contreras, R.; Armas, O. Performance, combustion timing and emissions from a light duty vehicle at different altitudes fueled with animal fat biodiesel, GTL and diesel fuels. *Appl. Energy* **2016**, *182*, 507–517. [CrossRef]
14. Wang, X.; Yin, H.; Ge, Y.; Yu, L.; Xu, Z.; Yu, C.; Shi, X.; Liu, H. On-vehicle emission measurement of a light-duty diesel van at various speeds at high altitude. *Atmos. Environ.* **2013**, *81*, 263–269. [CrossRef]
15. Wang, H.; Ge, Y.; Hao, L.; Xu, X.; Tan, J.; Li, J.; Wu, L.; Yang, J.; Yang, D.; Peng, J.; et al. The real driving emission characteristics of light-duty diesel vehicle at various altitudes. *Atmos. Environ.* **2018**, *191*, 126–131. [CrossRef]
16. Giraldo, H.; Huertas, J. I. Real emissions, driving patterns and fuel consumption of in-use diesel buses operating at high altitude. *Transp. Res. D* **2019**, *77*, 21–36. [CrossRef]
17. McCaffery, C.; Zhua, H.; Li, C.; Durbin, T. D.; Johnson, K. C.; Jung, H.; Brezny, R.; Geller, M.; Karavalakis, G. On-road gaseous and particulate emissions from GDI vehicles with and without gasoline particulate filters (GPFs) using portable emissions measurement systems (PEMS). *Sci. Total Environ.* **2020**, *710*, 136366. [CrossRef] [PubMed]

18. Gao, J.; Tian, A.; Sorniotti, G.; Karci, A.E.; Di Palo, R. Review of thermal management of catalytic converters to decrease engine emissions during cold start and warm up. *Appl. Therm. Eng.* **2019**, *147*, 177–187. [CrossRef]
19. Yusuf, A.A.; Inambao, F.L. Effect of cold start emissions from gasoline-fueled engines of light-duty vehicles at low and high ambient temperatures: Recent trends. *Case Stud. Therm. Eng.* **2019**, *14*, 100417. [CrossRef]
20. Arnau, F.J.; Martín, J.; Piqueras, P.; Auñón, Á. Effect of the exhaust thermal insulation on the engine efficiency and the exhaust temperature under transient conditions. *Int. J. Engine Res.* **2020**. [CrossRef]
21. Serrano, J.R.; Arnau, F.J.; Martín, J.; Auñón, Á. Development of a variable valve actuation control to improve diesel oxidation catalyst efficiency and emissions in a light duty diesel engine. *Energies* **2020**, *13*, 4561. [CrossRef]
22. Serrano, J.R.; Piqueras, P.; De La Morena, J.; Ruiz, M.J. Influence of pre-turbine small-sized oxidation catalyst on engine performance and emissions under driving conditions. *Appl. Sci.* **2020**, *10*, 7714. [CrossRef]
23. Hamedi, M.R.; Doustdar, O.; Tsolakis, A.; Hartland, J. Thermal energy storage system for efficient diesel exhaust aftertreatment at low temperatures. *Appl. Energy* **2019**, *235*, 874–887. [CrossRef]
24. Nicholas, M.; Tal, G.; Turrentine, T. Advanced plug-in electric vehicle travel and charging behavior. In Proceedings of the Advanced Clean Cars Symposium: The Road Ahead, California Environmental Protection Agency, Air Resources Board, Sacramento, CA, USA, 27–28 September 2016.
25. Piqueras, P.; García, A.; Monsalve-Serrano, J.; Ruiz, M.J. Performance of a diesel oxidation catalyst under diesel-gasoline reactivity controlled compression ignition combustion conditions. *Energy Convers. Manag.* **2019**, *196*, 18–31. [CrossRef]
26. Guardiola, C.; Pla, B.; Bares, P.; Mora, J. An on-board method to estimate the light-off temperature of diesel oxidation catalysts. *Int. J. Engine Res.* **2018**, *21*, 1480–1492. [CrossRef]
27. Peitz, D.; Elsener, M.; Kröcher, O. Impact of Catalyst Geometry on Diffusion and Selective Catalytic Reduction Kinetics under Elevated Pressures. *Chem. Ing. Tech.* **2018**, *90*, 795–802. [CrossRef] [PubMed]
28. Christensen, S.R.; Hansen, B.B.; Pedersen, K.H.; Thøgersen, J.R.; Jensen, A.D. Selective Catalytic Reduction of NOx over V2O5-WO3-TiO2 SCR Catalysts—A Study at Elevated Pressure for Maritime Pre-turbine SCR Configuration. *Emission Contr. Sci. Technol.* **2019**, *5*, 263–278. [CrossRef]
29. Peng, P.Y.; Harold, M.P.; Luss, D. Sustained concentration and temperature oscillations in a diesel oxidation catalyst. *Chem. Eng. J.* **2019**, *5*, 263–278. [CrossRef]
30. Boerensen, C.; Roemer, D.; Nederlof, C.; Smirnov, E.; Linzen, F.; Goebel, F.; Carberry, B. Twin-LNT System for Advanced Diesel Exhaust Gas Aftertreatment. *SAE Int. J. Fuels Lubr.* **2017**, *10*, 619–633. [CrossRef]
31. Oh, S.H.; Cavendish, J.C. Transients of monolithic catalytic converters response to step changes in feedstream temperature as related to controlling automobile emissions. *Ind. Eng. Chem. Prod. Res. Dev.* **1982**, *21*, 29–37. [CrossRef]
32. Serrano, J.R.; Piqueras, P.; Sanchis, E.J.; Diesel, B. A modelling tool for engine and exhaust aftertreatment performance analysis in altitude operation. *Results Eng.* **2019**, *4*, 100054. [CrossRef]
33. Desantes, J.M.; Galindo, J.; Payri, F.; Piqueras, P.; Serrano, J.R. Device for Atmosphere Conditioning for Testing Combustion Engines, and Associated Method and Use. Patent WO 2015/110683 A1, 30 July 2015.
34. Desantes, J.M.; Galindo, J.; Payri, F.; Piqueras, P.; Serrano, J.R. Device for Conditioning the Atmosphere in Test of Alternative Internal Combustion Engines, Method and Use of Said Device. Patent WO 2016/116642 A1, 28 July 2016.
35. Chundru, V.R.; Parker, G.G.; Johnson, J.H. Development of a Kalman filter estimator for simulation and control of NOx and PM in a SCR catalyst on a DPF. *Int. J. Engine Res.* **2020**. [CrossRef]
36. Galindo, J.; Serrano, J.R.; Piqueras, P.; Gómez, J. Description and performance analysis of a flow test rig to simulate altitude pressure variation for internal combustion engines testing. *SAE Int. J. Engines* **2014**, *7*, 1686–1696. [CrossRef]
37. Broatch, A.; Bermúdez, V.; Serrano, J.R.; Tabet-Aleixandre, R.; Gómez, J.; Bender, S. Analysis of passenger car turbocharged diesel engines performance when tested at altitude and of the altitude simulator device used. In Proceedings of the ASME 2018 Internal Combustion Engine Division Fall Technical Conference, San Diego, CA, USA, 4–7 November 2018.
38. Payri, F.; Arnau, F.J.; Piqueras, P.; Ruiz, M.J. Lumped Approach for Flow-Through and Wall-Flow Monolithic Reactors Modelling for Real-Time Automotive Applications. SAE Technical Paper 2018-01-0954; 2018. Available online: https://saemobilus.sae.org/content/2018-01-0954 (accessed on 23 December 2020).
39. Galindo, J.; Serrano, J.R.; Piqueras, P.; García Afonso, Ó. Heat transfer modelling in honeycomb wall-flow diesel particulate filters. *Energy* **2012**, *43*, 201–213. [CrossRef]
40. Serrano, J.R.; Piqueras, P.; De La Morena, J.; Sanchis, E.J. Late fuel post-injection influence on the dynamics and efficiency of wall-flow particulate filters regeneration. *Appl. Sci.* **2019**, *9*, 5384. [CrossRef]
41. Payri, F.; Bermúdez, V.R.; Tormos, B.; Linares, W.G. Hydrocarbon emissions speciation in diesel and biodiesel exhausts. *Atmos. Environ.* **2009**, *43*, 1273–1279. [CrossRef]
42. Tu, M.; Ratnakar, R.; Balakotaiah, V. Reduced order models with local property dependent transfer coefficients for real time simulations of monolith reactors. *Chem. Eng. J.* **2020**, *383*, 123074. [CrossRef]
43. Hawthorn, R.D. Afterburner catalysts effects of heat and mass transfer between gas and catalyst surface. *Am. Inst. Chem. Eng. Symp. Ser.* **1974**, *70*, 428–438.
44. Ratnakar, R.R.; Balakotaiah, V. Reduced order multimode transient models for catalytic monoliths with micro-kinetics. *Chem. Eng. J.* **2015**, *260*, 557–572. [CrossRef]

45. Voltz, S.E.; Morgan, C.R.; Liederman, D.; Jacob, S.M. Kinetic study of carbon monoxide and propylene oxidation on platinum catalysts. *Ind. Eng. Chem. Prod. Res. Dev.* **1973**, *12*, 294–301. [CrossRef]
46. Quiros, D.C.; Hu, S.; Hu, S.; Lee, E.S.; Sardar, S.; Wang, X.; Olfert, J.S.; Jung, H.S.; Zhu, Y.; Huai, T. Particle effective density and mass during steady-state operation of GDI, PFI, and diesel passenger cars. *J. Aerosol Sci.* **2015**, *83*, 39–54. [CrossRef]
47. Guardiola, C.; Pla, B.; Piqueras, P.; Mora, J.; Lefebvre, D. Model-based passive and active diagnostics strategies for diesel oxidation catalysts. *Appl. Therm. Eng.* **2017**, *110*, 962–971. [CrossRef]
48. Allen, C.M.; Joshi, M.C.; Gosala, D.B.; Shaver, G.M.; Farrell, L.; McCarthy, J. Experimental assessment of diesel engine cylinder deactivation performance during low-load transient operations. *Int. J. Engine Res.* **2019**. [CrossRef]
49. Suarez-Bertoa, R.; Valverde, V.; Clairotte, M.; Pavlovic, J.; Giechaskiel, B.; Franco, V.; Kregar, Z.; Astorga, C. On-road emissions of passenger cars beyond the boundary conditions of the real-driving emissions test. *Environ. Res.* **2019**, *176*, 108572. [CrossRef]
50. Lefort, I.; Herreros, J.M.; Tsolakis, A. Reduction of low temperature engine pollutants by understanding the exhaust species interactions in a diesel oxidation catalyst. *Environ. Sci. Technol.* **2014**, *48*, 2361–2367. [CrossRef] [PubMed]